Effects of Anthropogenic Aerosols on the East Asian Winter Monsoon

Shenglong Zhang[1,2], Jonathon S. Wright[1,2], Zengyuan Guo[2,3], Wenyu Huang[1,2], and Yiran Peng[1,2]

[1]Department of Earth System Science, Tsinghua University, Beijing, China

[2]Ministry of Education Key Laboratory for Earth System Modeling, Tsinghua University, Beijing, China

[3]Climate Studies Key Laboratory, National Climate Center, China Meteorological Administration, Beijing, China

Key Points:

- Anthropogenic aerosols make East Asian land areas roughly 1.5°C colder during winter while reducing precipitation and increasing snowfall
- Aerosol effects are diagnosed by analyzing how changes in diabatic heating alter the winter monsoon potential vorticity intrusion
- Colder surface temperatures can be attributed to both aerosol direct effects and circulation responses to cloud-aerosol interactions

Corresponding author: Jonathon S. Wright, jswright@tsinghua.edu.cn

Abstract

Circulation patterns linked to the East Asian winter monsoon (EAWM) affect precipitation, surface temperature, and air quality extremes over East Asia. These circulation patterns can in turn be influenced by aerosol radiative and microphysical effects through diabatic heating and its impacts on atmospheric vorticity. Using global model simulations, we investigate the effects of anthropogenic aerosol emissions and concentration changes on the intensity and variability of the EAWM. Comparison with reanalysis products indicates that the model captures the mean state of the EAWM well. The experiments indicate that anthropogenic aerosol emissions strengthen the Siberian High but weaken the East Asian jet stream, making the land areas of East Asia colder, drier, and snowier. Aerosols reduce mean surface air temperatures by approximately 1.5°C, comparable to about half of the difference between strong and weak EAWM episodes in the control simulation. The mechanisms behind these changes are evaluated by analyzing differences in the potential vorticity budget. Anthropogenic aerosol effects on diabatic heating strengthen anomalous subsidence over southern East Asia, establishing an anticyclonic circulation anomaly that suppresses deep convection and precipitation. Aerosol effects on cloud cover and cloud longwave radiative heating weaken stability over the eastern flank of the Tibetan Plateau, intensifying upslope flow along the western side of the anticyclone. Both circulation anomalies contribute to reducing surface air temperatures through regional impacts on thermal advection and the atmospheric radiative balance.

Plain Language Summary

The East Asian winter monsoon is a large-scale circulation system that controls the occurrence of cold air outbreaks and severe winter storms throughout the densely populated land areas of East Asia. By reducing the amount of sunlight reaching the surface, warming the atmosphere, and changing the properties and lifetimes of clouds, aerosols can alter the atmospheric circulation and regional weather conditions. Here, we examine the characteristics of the East Asian winter monsoon in global model simulations with and without aerosol emissions from industry, energy generation, transportation, and other human activities. Our results show that the aerosols produced by these activities make East Asian land areas colder, drier, and snowier during winter. We explain the reasons for these changes by diagnosing how various physical effects of aerosols impact temperature and winds within the East Asian monsoon region.

1 Introduction

The East Asian winter monsoon (EAWM) is a crucial component of the boreal wintertime climate system (L. Wang et al., 2009; L. Wang & Chen, 2010; Miao, Wang, Wang, Zhu, & Sun, 2018). Variations in the EAWM modulate wintertime precipitation, surface air temperature, and air quality in East Asia (W. Huang et al., 2016; Ge et al., 2019), and severe winter weather associated with these variations can have substantial socioeconomic impacts (R. Huang et al., 2003, 2007; B. Wang et al., 2000; Chang et al., 2006; H. Wang et al., 2011). The influences of a strong EAWM, which can extend from polar regions to the equator (Li et al., 2020), are typically characterized by a strengthened Siberian High and Aleutian Low at the surface, pronounced northerly winds along the coast of East Asia in the lower troposphere, a deeper East Asian trough in the middle troposphere, and a stronger jet stream in the upper troposphere over East Asia (L. Wang & Chen, 2010; Jiang et al., 2017; Li et al., 2020; Miao & Jiang, 2021).

These circulation components of EAWM are inherently linked. The Siberian High is established largely by the joint effects of strong radiative cooling and subsidence upwind of the East Asian trough (L. Wang et al., 2009). Cold air sweeps into southern China when the Siberian High strengthens and moves southeastward, leading to cold surges (Q. Guo, 1994; Fan, 2009; H. Wang et al., 2011). Cold air that peels off of the Siberian High can

also move into the tropical margins near the maritime continent, sharpening the meridional temperature gradient (Chang et al., 2005; L. Wang et al., 2009; Li et al., 2020) and intensifying deep convection and precipitation over Southeast Asia (Chang et al., 2005). Heat and moisture sourced from the warm tropical and subtropical ocean surface can thus serve as heating sources to the EAWM (Chang et al., 2006), enhancing baroclinicity (Blackmon et al., 1977) and triggering interactions between the tropics and midlatitudes (Chang & Lau, 1980, 1982; Compo et al., 1999). Variations in baroclinicity associated with the EAWM are also linked to jet dynamics in the upper troposphere, including variations in both the East Asian polar front jet and East Asian subtropical jet (Jhun & Lee, 2004; Luo & Zhang, 2015; Yin & Zhang, 2021).

Many indices have been proposed to describe variations in the EAWM (L. Wang & Chen, 2010; He & Wang, 2012; W. Huang et al., 2016; Li et al., 2020). Owing to evident links between EAWM intensity and the regional circulation, most of these index definitions have relied on dynamical variables rather than thermal variables (L. Wang & Chen, 2010). W. Huang et al. (2016) proposed a novel EAWM index based on potential vorticity (PV), which includes both dynamical (vorticity) and thermodynamic (thermal stratification) metrics of the atmospheric state. They pointed out that the EAWM essentially brings cold air along isentropic surfaces from the high latitude upper troposphere to the mid-latitude lower troposphere. This link can be described effectively as a southward intrusion of large values of PV. A strong PV intrusion indicates anomalous southward descent of the upper-level polar front along sharply sloping isentropic surfaces above East Asia. W. Huang et al. (2016) showed that a PV-based EAWMI reliably captures relationships between the EAWM and the Siberian High, Artic Oscillation, and El Niño–Southern Oscillation.

A stronger EAWM corresponds to negative anomalies in surface air temperature and a greater frequency of severe winter weather, including intense snowfall and cold surges over East Asia (Q. Guo, 1994; Fan, 2009; H. Wang et al., 2011), increased rainfall over the maritime continent (Chang et al., 2005), and decreased precipitation over South China (Zhou, 2011; Zhou & Wu, 2010). Surface air temperature anomalies over East Asia are often divided into a northern mode and a southern mode to account for the two distinct pathways by which cold air invades East Asia (B. Wang et al., 2010; Li et al., 2020). The northern mode represents cold air from central Siberia, leading to cold temperatures over northern East Asia, while the southern mode represents cold air from western Mongolia, leading to cold temperatures over southern East Asia.

The EAWM is affected by both natural and anthropogenic climate forcings (Chen & Zhang, 2013; Ding et al., 2007; Hori & Ueda, 2006; Hu et al., 2000; Lee et al., 2013; Miao, Wang, Wang, & Gao, 2018; Miao, Wang, Wang, Zhu, & Sun, 2018). For example, Miao, Wang, Wang, and Gao (2018) found that solar variability can regulate EAWM intensity through North Atlantic sea surface temperatures on the multidecadal time scale. Model simulations have also shown that fluctuations in natural external forcing play a key role in regulating meridional shear of the East Asian jet stream (Miao, Wang, Wang, Zhu, & Sun, 2018). In addition, a wealth of research has concluded that greenhouse gas-driven global warming weakens the EAWM (Ding et al., 2007; Hori & Ueda, 2006; Hu et al., 2000; Lee et al., 2013; Xu et al., 2016). Large-scale urbanization has also weakened the EAWM across much of East Asia, but with opposite effects on the EAWM in northeastern China (Chen & Zhang, 2013).

The rapid pace of economic development in East Asia over recent decades has dramatically increased regional emissions of anthropogenic aerosols and aerosol precursors. These emissions have resulted in a well-known weakening of the East Asian summer monsoon (Jiang et al., 2013; L. Guo et al., 2013; Song et al., 2014; Wei et al., 2022; Zhang et al., 2012). However, despite clear links between EAWM variability and air quality (Ge et al., 2019), few studies have examined the effects exerted by anthropogenic aerosols on the EAWM. Y. Liu et al. (2009) reported that sulfate tends to weaken the winter mon-

soon circulation in southeast China, while Wu et al. (2016) emphasized the potential for anthropogenic aerosols to weaken the monsoon circulation by reducing land–sea temperature contrasts. Previous studies have also found that black carbon can intensify the EAWM northern mode (characterized by a northward shift of the subtropical jet) via black carbon-induced warming of the Tibetan Plateau (Jiang et al., 2017). Another recent study found that the combined effects of anthropogenic and natural external forcings, including aerosols, weakened the Siberian High in the mid-1980s (Miao, Wang, Wang, Zhu, & Sun, 2018).

However, the magnitude and mechanisms of anthropogenic aerosol effects on the EAWM are still unclear. In this study, we use global model simulations to investigate the effects of anthropogenic aerosol emissions on the EAWM between 1999 and 2018. We use a PV-based EAWM index to provide both dynamical and thermodynamic perspectives, focusing on the ways in which anthropogenic aerosols alter diabatic heating over East Asia during wintertime. The paper is organized as follows. In section 2, we introduce the data and methods. In Section 3, we describe the simulated characteristics of the EAWM and the effects of anthropogenic aerosols on these characteristics. In section 4, we explore the mechanisms by which anthropogenic aerosols influence the EAWM. We close with a brief summary and discussion in section 5.

2 Data and Methods

2.1 Data

In this work, the EAWM is assessed using reanalysis products from the European Centre for Medium-Range Weather Forecasts (ECMWF) Fifth Reanalysis of the Atmosphere (ERA5; Hersbach et al., 2020) and global atmospheric model simulations from the Tsinghua University Community Integrated Earth System Model (CIESM; Lin et al., 2020). The ERA5 reanalysis products, which include monthly mean horizontal winds and temperatures on pressure levels and 2-meter surface air temperatures, are used to analyze the EAWM circulation and provide a benchmark for evaluating the model simulations. Winter is defined as November of the specified year through March of the following year (NDJFM).

2.2 Experimental design

The CIESM global model simulations have been conducted for the AeroCom Atmospheric Composition and Asian Monsoon (ACAM) experiment. The model is run at a horizontal resolution of 2.5° in longitude by approximately 1.875° in latitude (144×96) using a spectral element dynamical core with 30 hybrid σ-p vertical levels and a model top at 1 hPa. Land surface conditions are simulated using a modified version of the Community Land Model Version 4.0 (Lawrence et al., 2011) as described by Lin et al. (2020). Details of the atmospheric model physics are unchanged from those described by Lin et al. (2020), with the exception that prescribed aerosols are replaced by the interactive 7-mode Modal Aerosol Module (MAM7; X. Liu et al., 2012). Anthropogenic emissions through 2014 include estimates for the agricultural, energy, industrial, transportation, residential, waste, solvent production and application, international shipping, and aviation sectors based on version 2017-05-18 of the Community Emissions Data System (CEDS; Hoesly et al., 2018). Anthropogenic emissions from 2014 are repeated for the remaining years of each experiment (2015–2018). Volcanic emissions include estimates for eruptions and outgassing from Carn (2019). Fire emissions are from van Marle et al. (2017) for the years 1999–2015, with emissions from 2015 repeated annually for the years 2016–2018. Sea surface temperature and sea ice boundary conditions are applied as recommended for Atmospheric Model Intercomparison Project (AMIP) experiments by the Program for Climate Model Diagnosis and Intercomparison (Hurrell et al., 2008). The atmospheric model simulations are otherwise free-running, without meteorological nudging.

We use 6-hourly and monthly outputs from the control (BASE) and zero-anthropogenic (ANT0) aerosol emissions scenarios. Monthly-mean outputs from the BASE scenario, which represents historical changes in all emissions inventories, are compared with ERA5 to assess the ability of the CIESM to reliably simulate the basic characteristics of the EAWM. The ANT0 experiment includes volcanic and biomass burning emissions but excludes all emissions of anthropogenic aerosols and aerosol precursors. Anthropogenic aerosol effects are assessed as the difference between the ANT0 and BASE scenarios (BASE – ANT0). Daily averages of 6-hourly outputs from the BASE and ANT0 simulations are used to explore the mechanisms behind anthropogenic aerosol effects on the EAWM.

2.3 Methods

An EAWM index (EAWMI) is a metric that uses information from the wintertime circulation to quantitatively describe variations in the strength or other key aspects of the EAWM (L. Wang & Chen, 2010; He & Wang, 2012; W. Huang et al., 2016; Li et al., 2020). In this article, we use a modified version of the EAWMI proposed by W. Huang et al. (2016), which is based on potential vorticity (PV):

$$\mathrm{PV} = -g(\zeta + f)\frac{\partial \theta}{\partial p}, \tag{1}$$

where g is the gravitational acceleration, ζ is relative vorticity, f is the planetary vorticity, and θ is potential temperature. As shown by W. Huang et al. (2016), the PV-based EAWMI reliably captures relationships between the EAWM and other large-scale climate modes. Owing to its dependence on planetary vorticity (f) and stratification ($-\partial\theta/\partial p$), PV increases with both increasing latitude and increasing altitude. As PV is conserved for adiabatic frictionless flow, larger values of PV in the lower and middle troposphere over East Asia indicate an intrusion of cold, dry air from higher latitudes and altitudes. Further power derives from the invertibility of PV (Hoskins et al., 1985), which links the distribution of PV to the balanced wind and mass fields, and the PV tendency equation, which links diabatic heating and other non-conservative processes to changes in PV.

To limit noise due to frictional effects in the surface layer, particularly over and around the Tibetan Plateau, we define a modified PV-based EAWMI as follows:

$$\mathrm{EAWMI} = \overline{\mathrm{PV}^{m}_{300\mathrm{K}}(90°\mathrm{E}-150°\mathrm{E}, 20°\mathrm{N}-50°\mathrm{N})} - \overline{\mathrm{PV}^{m}_{300\mathrm{K}}(0-360°\mathrm{E}, 20°\mathrm{N}-50°\mathrm{N})}. \tag{2}$$

Here, $\mathrm{PV}^{m}_{300\mathrm{K}}$ is masked when pressure on the 300 K isentropic surface exceeds a reference pressure, for example:

$$p_{\mathrm{ref}} = p_{\mathrm{surf}} - dp. \tag{3}$$

The reference pressure can also be set directly to the pressure at the diagnosed boundary layer top (p_{ABL}). Values of the modified EAWMI with dp set to 60 hPa, dp set to 100 hPa, and p_{ref} set to p_{ABL} are highly correlated ($r \geq 0.97$). Given this consistency in the results and to avoid dependence on the method by which the boundary layer top is defined or diagnosed, we adopt equation 3 with dp =60 hPa to define the mask. Figure 1 shows the mean seasonal cycle of the EAWMI (Fig. 1a) and time series of the 5-day mean deseasonalized EAWMI (Fig. 1b) for the winters of 1999 to 2018 in the BASE and ANT0 simulations. The EAWMI for the BASE simulation has been standardized to have a mean of zero and a standard deviation of one. The EAWMI for the ANT0 simulation has been standardized against the reference mean and standard deviation from BASE to better indicate differences between the two simulations. Seasonal cycles for both

simulations are based on the first three Fourier components of the 151-day season averaged over the 19 full winters (November–March) in each simulation.

A larger value of the EAWMI indicates a stronger EAWM, associated with an intensified Siberian high and stronger northerly winds over the coastal areas of East Asia (W. Huang et al., 2016, 2017). Figure 1 therefore indicates that anthropogenic aerosol emissions strengthen the EAWM overall (Fig. 1a, right panel), with a shift in the distribution of daily-mean EAWMI from small negative values (−1 to 0) toward small positive values (0 to +1). Intensification of the EAWM is mainly confined to early (December) and late (March) winter, offset by a mid-winter weakening of the EAWM in BASE relative to ANT0 (Fig. 1a, left panel). These aerosol effects on the EAWM are explored further in the following sections.

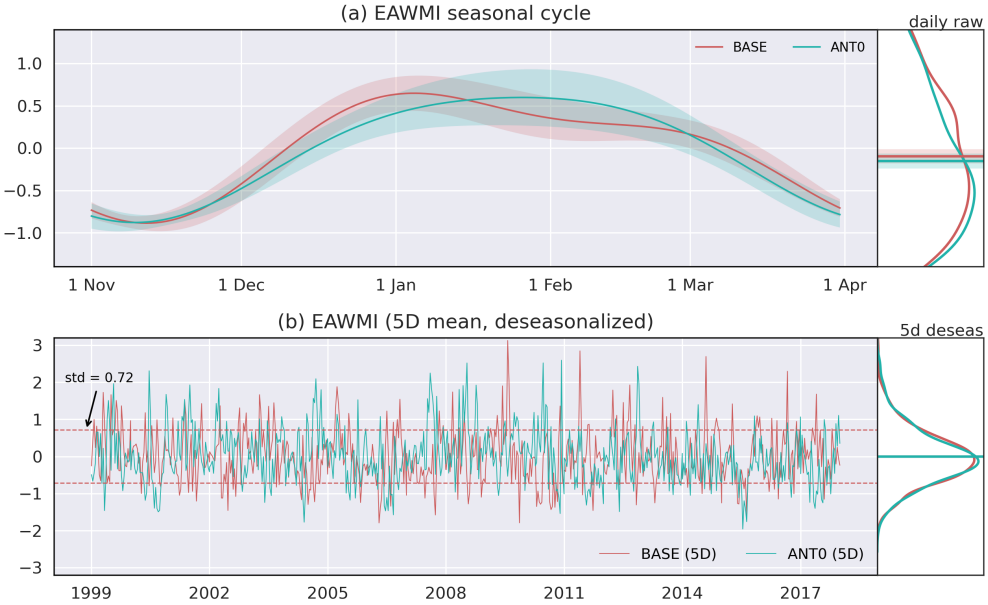

Figure 1. (a) Mean seasonal evolution of the EAWMI from 1 November to 31 March and (b) rolling 5-day mean deseasonalized EAWMI for November–March of 1999–2018 from the BASE and ANT0 simulations. Distributions at right are shown for the raw daily standardized time series (without deseasonalization) and the 5-day-mean deseasonalized time series. Results from both simulations are standardized against the BASE mean and standard deviation.

To analyze the mechanisms by which anthropogenic aerosols affect the EAWM, we use the PV tendency equation in isentropic coordinates (Lackmann, 2012):

$$\frac{d\mathrm{PV}}{dt} = \mathrm{PV}\frac{\partial\dot{\theta}}{\partial\theta} + g\frac{\partial\theta}{\partial p}\left(\frac{\partial\dot{\theta}}{\partial x}\frac{\partial v}{\partial\theta} - \frac{\partial\dot{\theta}}{\partial y}\frac{\partial u}{\partial\theta}\right) + g\frac{\partial\theta}{\partial p}\left(\frac{\partial F_y}{\partial x} - \frac{\partial F_x}{\partial y}\right) \tag{4}$$

where $\dot{\theta}$ is diabatic heating, u and v are the zonal and meridional components of the horizontal wind, and F_x and F_y are frictional effects in the zonal (x) and meridional (y) directions, respectively. The terms on the right-hand side of equation 4 can be described as the vertical diabatic, shear diabatic, and frictional PV tendencies, respectively. We focus on changes in the two diabatic terms between the ANT0 and BASE simulations, which can be viewed as forcing imposed by aerosol effects on the circulation. Changes in the frictional term primarily represent spindown of the altered circulation.

3 Simulated mean state and changes in the EAWM

3.1 The EAWM mean state

Potential temperature (θ) is an indicator of atmospheric entropy and its vertical gradient is often used as a measure of static stability. Potential vorticity (PV) is proportional to the product of absolute vorticity and static stability. Both potential temperature and PV are conserved for adiabatic and frictionless processes. Latitude–pressure cross-sections of potential temperature and PV over the East Asian domain (90–150°E, 20–50°N) are illustrated in Figure 2a,e. The atmosphere has a strong baroclinic structure over mid-latitude East Asia during boreal winter, as indicated by sharply sloping potential temperature contours in latitude-pressure cross-sections (Fig. 2a). Values of PV increase both with increasing latitude and increasing altitude (Fig. 2e). The 300 K and 310 K potential temperature surfaces, which connect the upper troposphere in the northern part of the domain to the lower troposphere in the south, are shown for reference. The 2 PVU surface ($1\,\mathrm{PVU} = 1\times10^{-6}\,\mathrm{K\,m^2\,s^{-1}\,kg^{-1}}$) is often defined as the dynamical tropopause (Lackmann, 2012), locating the 310 K contour within the lowermost stratosphere at 40–50°N.

The characteristic PV intrusion associated with the EAWM is illustrated by calculating differences between the East Asian (90–150°E) and global zonal means. Compared with ERA5 (Fig. 2b, f), the CIESM BASE simulation captures the mean state of the EAWM well. In particular, the model reproduces positive potential temperature anomalies and negative PV anomalies in the upper troposphere ($p < 500$ hPa) over 20–30°N, as well as deep negative potential temperature anomalies and positive PV anomalies over 30–50°N (Fig. 2b, c, f, g). According to the thermal wind relation, the enhanced meridional gradient in potential temperature over East Asia (Fig. 2c) is associated with stronger positive vertical shear in the zonal wind. This enhanced vertical shear indicates a regionally enhanced subtropical westerly jet stream co-located with the largest PV gradient (Fig. 2e-g), the location of which can be readily obtained from PV inversion. Specifically, positive PV anomalies over 30–50°N indicate enhanced cyclonic shear vorticity relative to the zonal mean, while negative PV anomalies over 20–30°N indicate enhanced anticyclonic shear vorticity. This PV pattern suggests the presence of stronger westerlies centered at the zero line (Fig. 2f-g). The EAWM produces relatively cold surface air temperatures in comparison to the zonal mean (Fig. 2j-k), particularly in the northern part of the domain. As with the distributions of potential temperature and PV, the CIESM (Fig. 2k) reliably reproduces the regional surface air temperature anomalies indicated by ERA5 (Fig. 2j).

The effects of anthropogenic aerosols shift the largest positive PV anomalies northward, as illustrated by the BASE–ANT0 difference in Figure 2h. Aerosol effects likewise move the cyclonic wind anomalies northward, indicating a weakening of the subtropical jet stream. Positive differences in potential temperature aloft and negative differences in potential temperature near the surface indicate a colder lower troposphere and enhanced static stability over 30–50°N (Fig. 2d). Surface air temperatures are also reduced over the entire EAWM region when emissions of anthropogenic aerosols and aerosol precursors are included in the model (Fig. 2l).

3.2 Effects of anthropogenic aerosols on the EAWM

In addition to the southward PV intrusion, a strong EAWM is usually associated with a more intense cold Siberian High and warm Aleutian Low at the surface, a stronger East Asian major trough in the middle troposphere, and a stronger subtropical jet stream in the upper troposphere (L. Wang & Chen, 2010; Jiang et al., 2017; Li et al., 2020; Miao & Jiang, 2021). Figure 3 shows monthly surface pressure (PS), 500 hPa geopotential height (Z500), and 200 hPa zonal winds (U200) regressed onto the PV-based EAWMI. A strong EAWM is associated with positive surface pressure anomalies at middle and high lat-

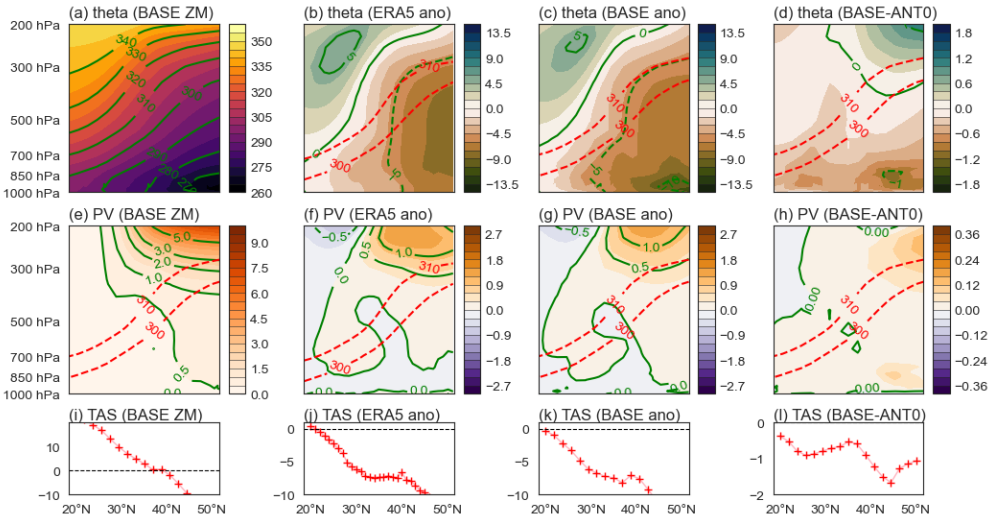

Figure 2. (a, e, i) East Asian zonal mean potential temperature (θ, K), potential vorticity (PV, PVU), and surface air temperature (TAS, ℃) from BASE (left); differences between the East Asian (90–150°E) and global zonal means (b, f, j) from ERA5 (left center) and (c, g, k) BASE (right center); and (d, h, l) differences between BASE and ANT0 (right) for November–March of 1999–2018.

itudes over Eurasia, including a southward extension into East Asia (Fig. 3a). This distribution of surface pressure anomalies indicates a stronger Siberian High and northerly flow in the coastal regions of East Asia. A stronger EAWM is also associated with a center of low surface pressure east of Japan, as indicated by negative surface pressure anomalies over the western North Pacific (Fig. 3a). Negative anomalies in 500 hPa geopotential height over northeast China and Japan indicate that a stronger EAWM is associated with a deeper East Asian trough, which increases the supply of cold air to the North Pacific (L. Wang et al., 2009). Positive 200 hPa zonal wind anomalies over East Asia and the North Pacific around 20–40°N show that the westerly jet in that region is enhanced when the EAWM is strong (Fig. 3c).

The effects of anthropogenic aerosols on the EAWM are further explored by calculating differences in surface pressure, 500 hPa geopotential height, and 200 hPa zonal wind between the BASE and ANT0 simulations. Anthropogenic aerosols induce positive surface pressure anomalies over parts of Mongolia and China, indicating that aerosol effects strengthen the southern part of the Siberian High. The Aleutian Low is shifted southward and eastward in the BASE simulation relative to ANT0, as indicated by negative surface pressure differences around 20–40°N over the North Pacific and positive differences to the north (Fig. 3b). Negative anomalies in mid-tropospheric geopotential height move northward and westward when aerosol effects are included (Fig. 3d). These negative anomalies indicate a weak northwestward extension of the East Asian trough, which increases the likelihood for cold air to sweep into north China and southeast Asian. In the upper troposphere, negative anomalies in zonal wind located in the climatological jet core region indicate that aerosols weaken the East Asian westerly jet (Fig. 3f). Positive anomalies to the south indicate a companion weakening of the tropical easterlies.

To summarize, aerosols strengthen the Siberian High, weaken the Aleutian Low, extend the East Asian trough northwestward, and weaken the East Asian jet stream. Among these changes, the first and third are consistent with a stronger EAWM, while the second and fourth are not (cf. left column of Fig. 3). Miao, Wang, Wang, Zhu, and Sun (2018)

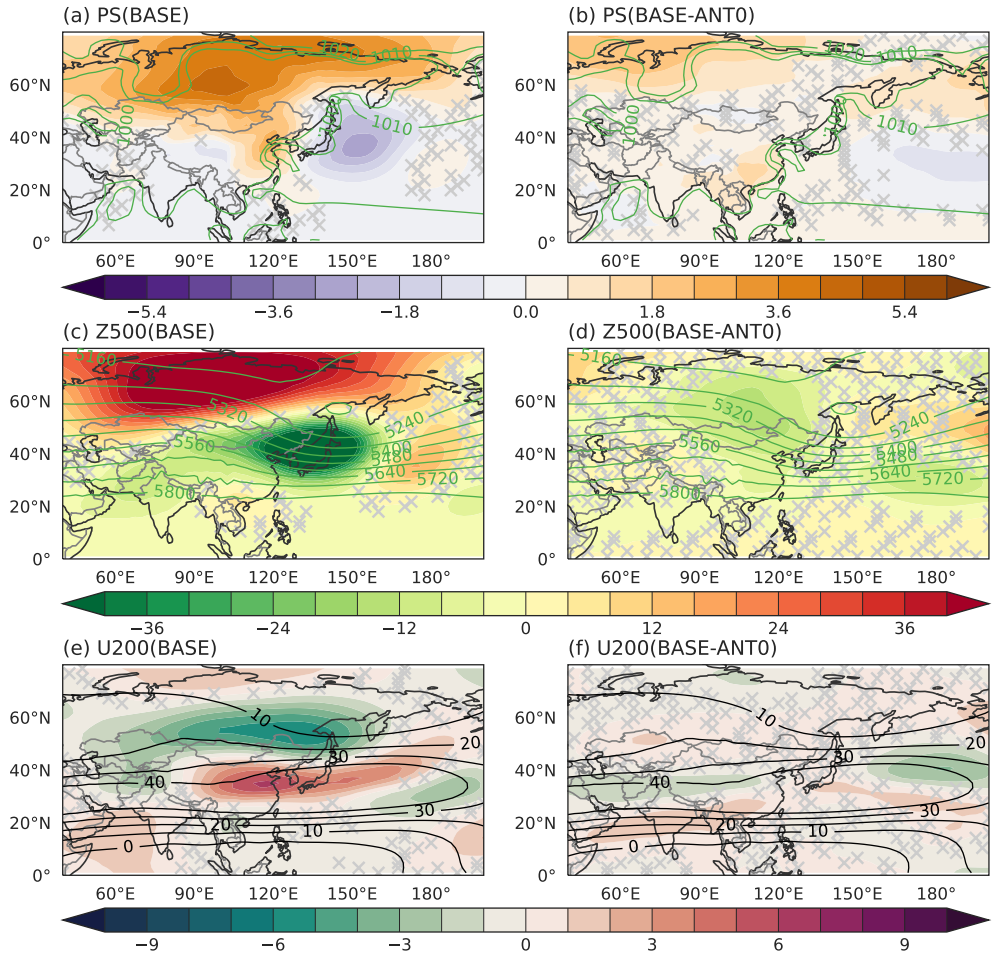

Figure 3. Anomalies in (a) surface pressure (PS, hPa), (c) 500 hPa geopotential height (Z500, m), and (e) 200 hPa zonal wind (U200; $\mathrm{m\,s^{-1}}$) from the BASE simulation regressed onto the deseasonalized and standardized PV-based EAWMI time series; and differences in (b) PS, (d) Z500, and (f) U200 between the BASE and ANT0 scenarios for November–March of 1999–2018. Contours in (a)-(f) denote the corresponding climatology. Hatching denotes where anomalies or differences are not significant at the 95% or greater confidence level based on Student's t test.

also found that anthropogenic forcings can play different roles at different pressure levels in modulating the intensity of the EAWM. These inconsistencies can be attributed at least in part to the strong baroclinicity over East Asia and the ways that aerosols modify this thermodynamic structure. Traditional methods that measure the intensity of the EAWM through mutually correlated surface and isobaric circulation patterns are therefore not sufficient to analyze the response of the EAWM to anthropogenic aerosol effects. More generally, analyzing dynamical components alone provides an incomplete description of the EAWM, which has distinctive thermal characteristics that help to determine the patterns and temporal variability of temperature and precipitation anomalies over East Asia during wintertime.

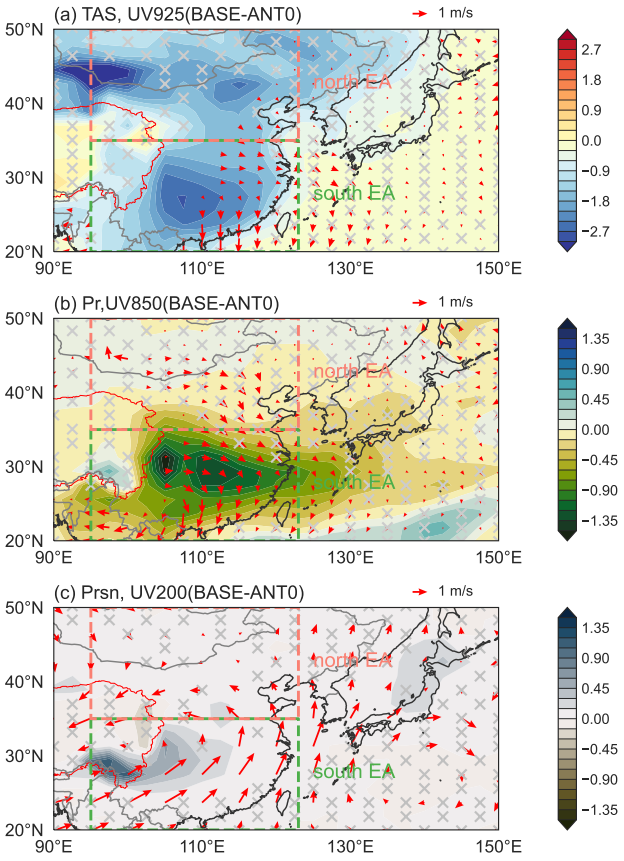

Figure 4. Differences in (a) mean surface air temperature (TAS, K), precipitation (Pr, mm d^{-1}), and snowfall (Prsn, mm d^{-1}) during November–March of 1999–2018 between the BASE and ANT0 scenarios. Hatching denotes locations where differences are not significant at the 95% or greater confidence level based on Student's t test (a) or the Mann-Whitney U test (b and c). Vectors indicate changes in horizontal winds on the 925 hPa (a), 850 hPa (b), and 200 hPa (c) isobaric surfaces. The domains assigned to the southern (20–35°N, 95–125°N) and northern (35–50°N, 95–125°N) parts of East Asian land areas are denoted by dashed rectangles labeled south-EA and north-EA, respectively.

To provide a more thermodynamic perspective on how anthropogenic aerosols alter the EAWM, Figure 4 shows differences in surface air temperature, total precipitation, and snowfall between the BASE and ANT0 simulations. These three variables are important indicators of the impacts of EAWM variability on severe winter weather and

human activities (Li et al., 2020). Surface air temperature provides an alternative measure of the intensity of the EAWM, while precipitation and snowfall represent dangers associated with the EAWM. To better analyze the impacts of anthropogenic aerosols, we divide the land areas of East Asia into southern (20–35°N, 95–125°E) and northern (35–50°N, 95–125°E) domains. Anthropogenic aerosol effects make the southern domain colder, drier, and snowier, as indicated by decreases in surface air temperature and total precipitation and increases in snowfall in the BASE simulation relative to ANT0 (Fig. 4). Negative changes in surface air temperature are also simulated over the northern part of the domain, highlighting that anomalously cold air transits through the north on its way to the south. Weak increases in surface air temperature over the Tibetan Plateau may be associated with black carbon-induced warming effects as noted by Jiang et al. (2017). It is interesting that snowfall tends to increase over the southern part of East Asia when anthropogenic aerosol emissions are included in the model even though total precipitation decreases (Fig. 4b, c). These differences require further exploration; however, relative to the ANT0 case, anthropogenic aerosol emissions narrow negative θ anomalies around 35–50°N while expanding negative θ anomalies in the lower troposphere around 20–35°N and positive θ anomalies in the upper troposphere around 35–50°N (Fig. 2d). The largest decreases in potential temperature are located near the surface, indicating that aerosol effects increase static stability and suppress precipitation throughout East Asia. The effects of these changes are more pronounced in the southern domain, where wintertime precipitation is both more frequent and more abundant.

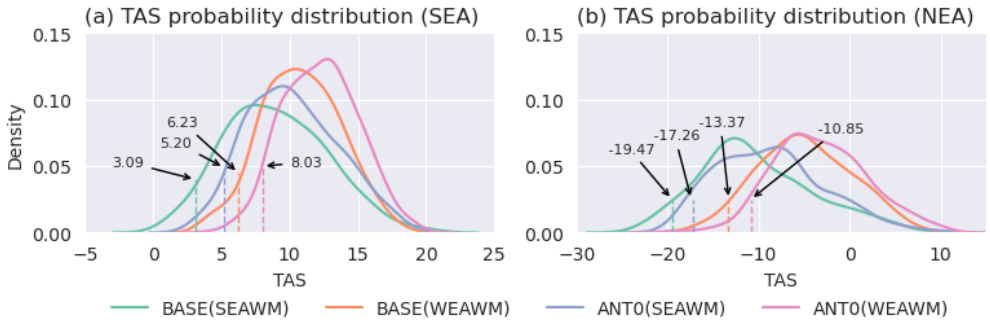

Figure 5. Surface air temperature (TAS, °C) probability distributions for strong and weak EAWM days over (a) south East Asian land areas (20–35°N, 95–125°N) and (b) north East Asian land areas (35–50°N, 95–125°N) during November–March of 1999–2018 under the BASE and ANT0 scenarios.

To quantitatively examine the effects of anthropogenic aerosols on surface air temperature, the distributions of surface air temperature for strong and weak EAWM days are computed and compared under different scenarios. Strong (weak) EAWM days are defined as days for which the deseasonalized EAWMI is greater (less) than one positive (negative) standard deviation from the mean, which is essentially zero for both simulations (Fig. 1b). As shown in Figure 5, the coldest 5% of days in the BASE simulation are on average 1.8–2.1°C colder in the southern domain and about 2.2–2.5°C colder in the northern domain than those in ANT0 during both strong and weak EAWM periods. These differences are equivalent to about 65% of the difference between strong and weak EAWM periods in the southern domain and about 38% of the difference between strong and weak EAWM periods in the northern domain. Moreover, area-weighted mean surface air temperatures are 1.51°C smaller over southern East Asia and 1.42°C smaller over northern East Asia in BASE relative to ANT0 (Fig. 4a). The above results suggest anthropogenic aerosols play an important role in modulating surface air temperature in winter time. Considering the close relationships between surface air temperature anoma-

lies and severe winter weather, these differences indicate that anthropogenic aerosols significantly heighten the risks associated with severe winter weather in East Asia.

4 Mechanisms behind anthropogenic aerosol effects on the EAWM

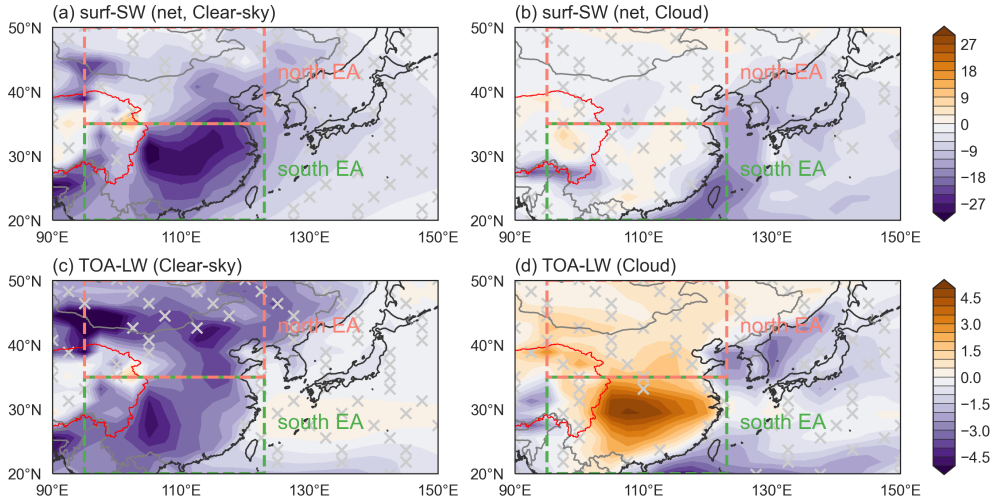

Figure 6. Spatial distributions of differences in (a) net clear-sky shortwave radiation flux at the surface, (b) cloud effects on net shortwave radiation flux at the surface, (c) upward clear-sky longwave flux at the top-of-atmosphere, and (d) cloud effects on upward longwave flux at the top-of-atmosphere between the BASE and ANT0 simulations. Hatching denotes locations where differences are not significant at the 95% or greater confidence level based on Student's t test. Net flux is calculated with downward flux minus upward flux. Units are Wm^{-2}.

Interactions among aerosols, radiation, and clouds play important roles in the climate system through their impacts on the surface energy budget, cloud physics, atmospheric heating, and the atmospheric water cycle (IPCC, 2021; Wu et al., 2016). We therefore analyze anthropogenic aerosol effects on the EAWM from an energetic perspective, focusing on how aerosols alter spatial distributions of radiative fluxes and diabatic heating. Figure 6 shows changes in the net downward flux of shortwave radiation at the surface and the upward flux of longwave radiation at the nominal top-of-atmosphere. Both clear-sky changes and changes in cloud effects (all-sky minus clear-sky) are shown to distinguish aerosol direct (aerosol-only) and indirect (aerosol–cloud) effects. Aerosols significantly reduce the flux of solar radiation reaching the surface throughout East Asia (Fig. 6a), with all-sky area-mean time-mean changes of $-23.7\,\mathrm{W\,m^{-2}}$ in the northern East Asia domain and $-11.5\,\mathrm{W\,m^{-2}}$ in the southern East Asia domain. In both the northern and southern domains, approximately 40–45% of the decrease in solar radiation flux at the surface is attributable to increased atmospheric absorption, with the remainder attributable to increases in planetary albedo. Outside of some pockets along the eastern flank of the Tibetan Plateau and the southeastern coast of China, cloud effects on net surface solar radiation are small over the land areas of East Asia (Fig. 6b). Reduced surface insolation is therefore mainly attributable to aerosol direct effects. Outgoing longwave radiation under clear-sky conditions is reduced in BASE relative to ANT0 over most of the EAWM region, as expected given colder temperatures (Fig. 6c). However, increases in all-sky longwave radiation are simulated over the Yangtze River valley in the southern East Asia domain due to changes in the cloud longwave effect (Fig. 6d). These changes are associated with decreases in high cloud cover and increased longwave emission from

low clouds, as discussed below. Aerosol–cloud interactions thus enhance the loss of energy by longwave radiation over southern East Asia (area mean: $+1.1\,\mathrm{W\,m^{-2}}$), partially offsetting the reduction in clear-sky OLR ($-2.6\,\mathrm{W\,m^{-2}}$) associated with colder temperatures at the surface (Fig. 4a) and in the lower troposphere (Fig. 2d).

Figure 7 shows vertical profiles of differences in heating between the BASE and ANT0 scenarios, including radiative and non-radiative components. Aerosol effects on total heating include deep reduction in diabatic heating that extend from the surface to 300 hPa around 20–35°N, and positive heating anomalies in a shallow layer just above the surface and in the upper troposphere (Fig. 7f). The deep and strong reductions in heating in the lower and middle troposphere around 20–35°N suggest strong reductions in non-radiative heating (Fig. 7e), primarily because less precipitation means less latent heat release. By contrast, reduced heating in the lower troposphere around 35–50°N is mainly due to changes in cloud radiative effects on longwave heating (Fig. 7d). Increases in heating in the shallow layer above the surface can be attributed primarily to changes in clear-sky shortwave heating and cloud effects on longwave heating there (Fig. 7a-d). Increases in shortwave heating and decreases in longwave heating in the lower troposphere largely compensate each other, while increases in shortwave and longwave heating in the upper troposphere both contribute to intensifying total heating there (Fig. 7).

Anthropogenic aerosols increase absorption of shortwave radiation near the surface, particularly in locations where large aerosol concentrations are restricted to the boundary layer (Fig. 7a). With greater numbers of aerosols serving as cloud condensation nuclei, the absorption of solar radiation near the surface in cloudy areas decreases (Fig. 7b) owing to smaller droplet sizes and longer cloud lifetimes (i.e., aerosol indirect effects; Twomey, 1977; Ackerman et al., 1995; Li et al., 2022). Meanwhile, shortwave heating and longwave cooling increase near the tops of these enhanced cloud layers (Fig. 7b,d) owing to enhanced absorption and reflection of shortwave radiation and enhanced emission of longwave radiation, respectively. Here, we do not attempt to distinguish the individual impacts of various semi-direct and indirect effects, instead classing all changes in cloud amount and cloud radiative effects as 'indirect' (i.e., resulting from aerosol–cloud interactions).

Given the dryness of the winter monsoon, it is perhaps surprising that the most prominent impact of anthropogenic aerosols is expressed through changes in non-radiative heating (Fig. 7e), which collects diabatic heating components associated with moist convection, large-scale precipitation, and turbulent mixing. Contributions from turbulent mixing are small, so this non-radiative term is dominated by latent heat release associated with precipitation formation (Fig. 7e). The vertical structure of the change indicates reductions in the production of both large-scale precipitation in the lower troposphere (through, e.g., longer cloud lifetimes) and convective precipitation in the middle and upper troposphere (through, e.g., stabilization by aerosol shortwave absorption). These changes indicate that both the occurrence and development of wintertime precipitation in these simulations are greatly altered by anthropogenic aerosol effects.

Diabatic heating is closely related to vertical motion. Figure 8 shows differences in pressure vertical velocity (w) in longitude–pressure cross-sections averaged over 20–35°N and 35–50°N. Deep increases in pressure vertical velocity anomalies around 90–125°E over the southern part of East Asia (Fig. 8a) indicate substantial reductions of upward motion. The strong increase in sinking motion (Fig. 8a) over southern East Asia implies weaker convection and suppressed convective heating (Fig. 7e), and is consistent with significant decreases in precipitation over this region in BASE relative to ANT0 (Fig. 4b). The weak increase in sinking motion over northern East Asia (Fig. 8b) is consistent with shallower non-radiative heating anomalies (Fig. 7e) and relatively weaker reductions in precipitation there (Fig. 4b).

As shown in section 3.2, traditional metrics based on surface and isobaric circulation patterns provide inconsistent indications of how the EAWM is modified by anthro-

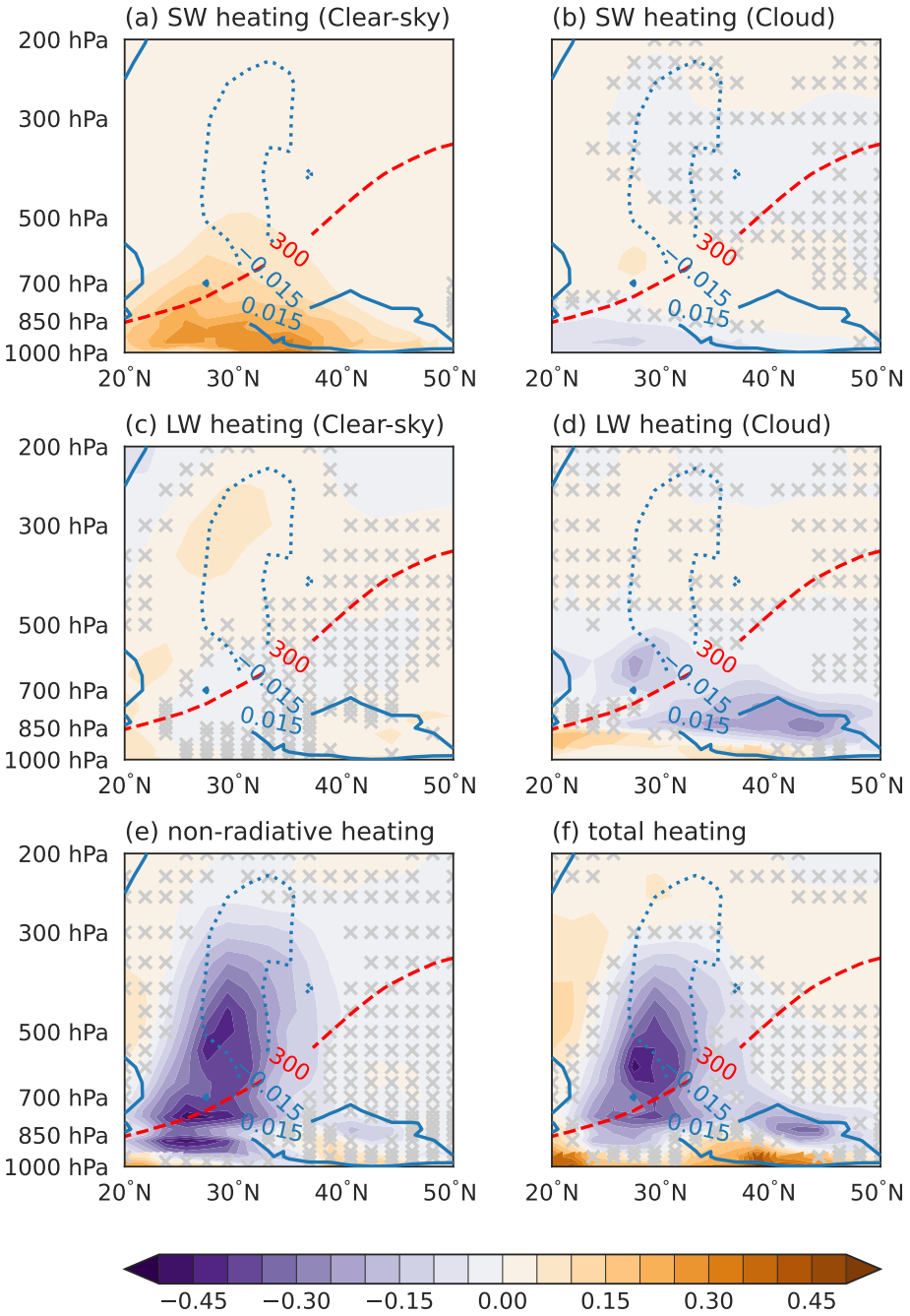

Figure 7. Latitude-pressure cross-sections of differences in (a) clear-sky shortwave radiative heating, (b) cloud shortwave radiative heating, (c) clear-sky longwave radiative heating, (d) cloud longwave radiative heating, (e) non-radiative heating, and (f) total heating ($\mathrm{K\,d^{-1}}$) averaged within 90–150°E between the BASE and ANT0 scenarios. Hatching denotes differences that are not significant at the 95% or greater confidence level based on Student's t test. Blue contours in all panels indicate changes in vertically resolved cloud area fraction, with negative changes indicated by dotted contours.

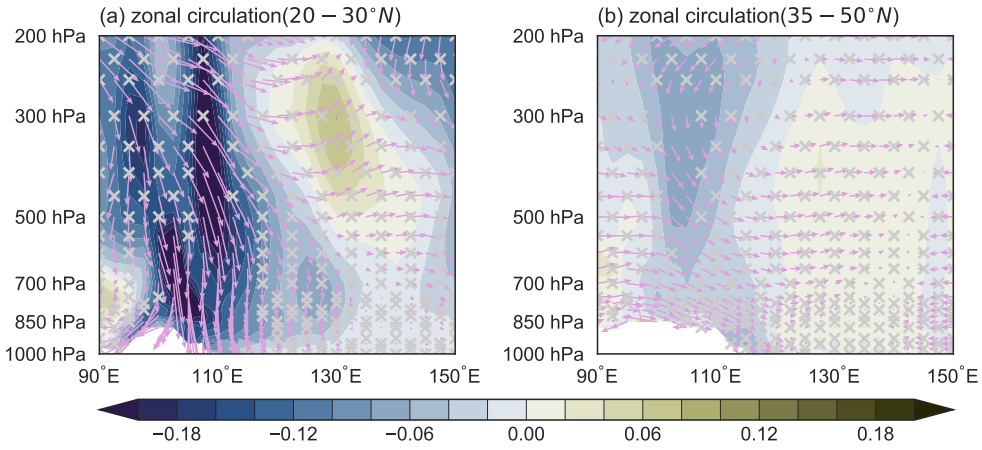

Figure 8. Longitude-pressure section of vertical velocity (shading, $\mathrm{cm\,s^{-1}}$) and the zonal overturning circulation (vectors) averaged within (a) 20–35°N and (b) 35–50°N. Hatching denotes locations where differences are not significant at the 95% or greater confidence level based on Student's t test.

pogenic aerosols. We therefore analyze changes in the EAWM from an isentropic PV perspective, which better accounts for coupled changes in thermal and dynamical variables. Figure 9 shows differences in PV and diabatic PV tendencies on the 300 K isentropic surface. Anthropogenic aerosols result in enhanced PV on this isentropic surface in the northern, southern, and western parts of the East Asian domain. These increases bracket an area of decreased PV over the Yangtze River Valley, consistent with an intensification of the mean distribution of EAWM-related PV anomalies relative to the zonal mean (see also Figure 2f-h). Changes in diabatic PV tendencies (i.e., the sum of vertical and shear diabatic PV tendencies in equation 4) are broadly similar to the changes in 300 K isentropic PV south of 40°N, with increases in the northwestern, western, and southern portions of the domain bracketing an area of decreases over central and eastern China.

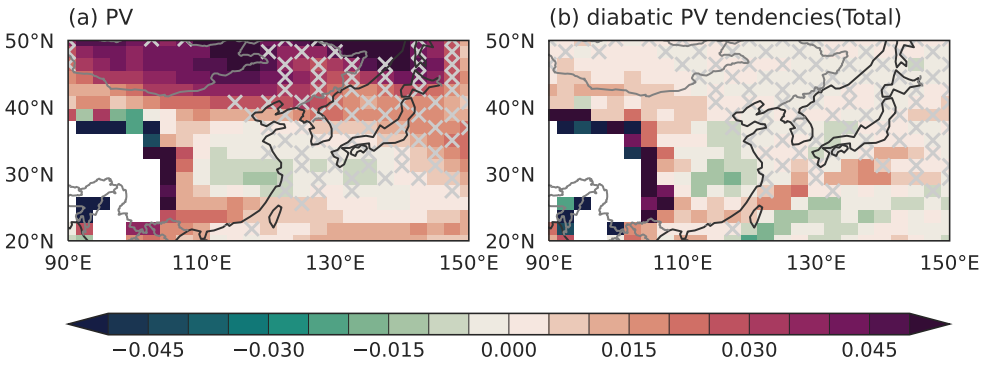

Figure 9. Differences in (a) potential vorticity (PV; units: PVU) and (b) time-mean diabatic contributions to PV tendencies (units: $\mathrm{PVU\,d^{-1}}$) on the 300 K isentropic level between the BASE and ANT0 simulations. Hatching denotes locations where differences are not significant at the 95% or greater confidence level based on Student's t test.

Figure 10 decomposes the changes in diabatic PV tendencies on the 300K isentropic level into individual components. The left column of this figure summarizes changes in the vertical diabatic PV tendency terms. Negative changes in PV over the Yangtze River Valley (Fig. 9a) indicate that anthropogenic aerosol effects weaken the PV intrusion in that part of the domain. Corresponding decreases in vertical diabatic PV tendencies (Fig. 10g) link this weakened PV intrusion to anthropogenic aerosol effects on diabatic heating, particularly the component due to non-radiative heating (Fig. 10e). Negative PV anomalies are associated with anticyclonic circulation anomalies in that region, favoring high pressures and suppressing deep convection (Fig. 8a). By contrast, increased vertical diabatic PV tendencies along the eastern flank of the Tibetan Plateau (Fig. 10g) include contributions from both non-radiative heating (Fig. 10e) and longwave radiative heating (Fig. 10c). The latter component is almost entirely attributable to cloud radiative effects, indicating that aerosol–cloud interactions make an important contribution to the response in this part of the domain. Increased PV tendencies due to changes longwave heating along the eastern flank of the Tibetan Plateau are partially compensated by reductions due to changes in shortwave heating in the same region (Fig. 10a). Unlike the longwave component, the shortwave contribution is almost entirely from changes in clear-sky heating. Examination of the vertical distribution of changes in total shortwave heating (Fig. 7a,b) shows that this reduction in the vertical diabatic PV tendency results from enhanced shortwave absorption below the 300 K level. The associated increase in vertical convergence of air from below acts to reduce PV locally. Increased PV along the eastern flank of the Tibetan Plateau indicates cyclonic circulation anomalies and decreased static stability. These changes are associated with topographically-forced uplift of relatively moist air along the western side of the anticyclonic circulation anomaly to the southeast, which acts to increase snowfall over the southeastern flank of the Plateau (Fig. 4c).

The right column of Figure 10 decomposes changes in total shear diabatic PV tendencies (Fig. 10h) into contributions from different physical parameterizations. Changes in shear diabatic PV tendencies associated with shortwave and longwave radiation are negligible (Fig. 10b,d), with changes in the total tendency almost entirely attributable to changes in the non-radiative component (Fig. 10f). Changes in this term largely oppose the changes due to the vertical diabatic term (Fig. 10e), especially over the Yangtze River Valley. Although changes in the shear diabatic term are smaller than those in the vertical diabatic term, compensation between these two terms nonetheless weakens the total decrease in PV over this region (Fig. 9). Increases in the non-radiative shear diabatic term around 110–150°E and 20–40°E are associated with strong wind shear and a sharp temperature gradient in the baroclinic zone above East Asia (Fig. 2). Enhanced stability in this region (Fig. 2d) inhibits convection and results in negative precipitation anomalies (Fig. 4b). By contrast, decreases in the non-radiative shear diabatic term over the western North Pacific (Fig. 10f) indicate weak wind shear and a weak temperature gradient. Changes in precipitation are positive over this far southeastern corner of the analysis domain (Fig. 4b).

To summarize, the anticyclonic anomaly over southern China in BASE relative to ANT0 (Fig. 3b, Fig. 4a-b) contributes to reducing surface air temperatures over both eastern and southwestern China (Fig. 4a), but by somewhat different mechanisms. The anomalous circulation contributes to colder surface temperatures over the Yangtze River Valley by strengthening northerly cold air advection along the coast (Fig. 4a-b) and reducing cloud cover, thereby intensifying longwave cooling to space (Fig. 6d). By contrast, upslope flow on the western flank of the anticyclone contributes to colder surface air temperatures over southwestern China by intensifying adiabatic cooling and snowfall (Fig. 4c). Associated increases in cloud cover further inhibit surface shortwave heating (Fig. 6b). Both sets of changes amplify the impacts of reduced surface insolation induced by the aerosol direct effect (Fig. 6a). By contrast, the lack of significant near-surface circulation changes over northeastern China (Fig. 3b, Fig. 4a) implies that reduced surface air

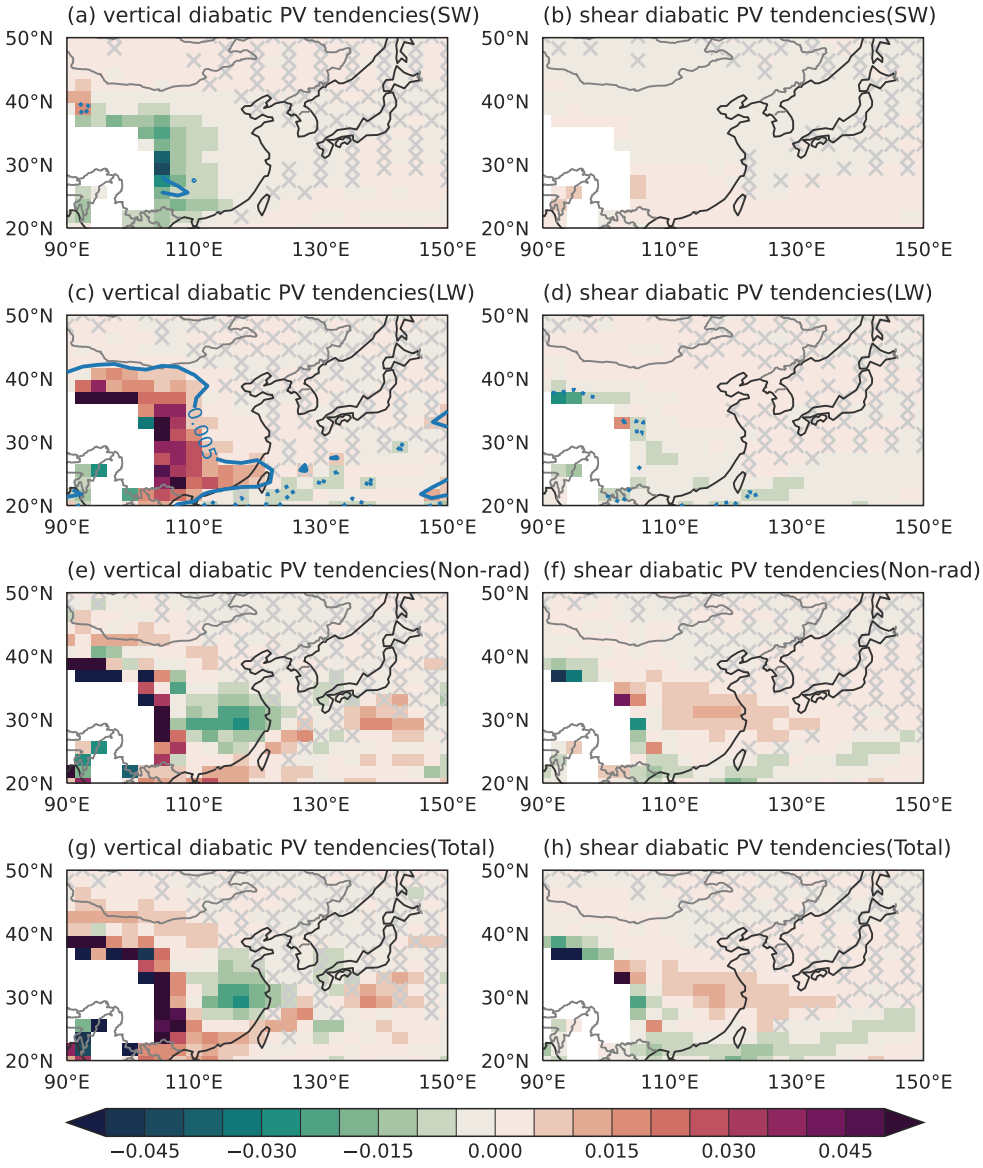

Figure 10. Differences in vertical diabatic PV tendencies (PV$\frac{\partial \dot{\theta}}{\partial \theta}$, PVU d^{-1}) associated with (a) shortwave radiative heating, (c) longwave radiative heating, (e) non-radiative heating, and (g) total heating and differences in shear diabatic PV tendencies ($g\frac{\partial \theta}{\partial p}\left(\frac{\partial \dot{\theta}}{\partial x}\frac{\partial v}{\partial \theta} - \frac{\partial \dot{\theta}}{\partial y}\frac{\partial u}{\partial \theta}\right)$, PVU d^{-1}) associated with (b) shortwave radiative heating, (d) longwave radiative heating, (f) non-radiative heating, and (h) total heating at the 300K isentropic level between the BASE and ANT0 scenarios. Values are masked where the 300K isentropic surface intersects the atmospheric boundary layer and hatching indicates where differences are not significant at the 95% or greater confidence level based on Student's t test. Blue contours in panels a-d indicate contributions from changes in cloud radiative effects.

temperatures there are primarily caused by the aerosol direct effect on surface insolation (Fig. 6a).

5 Conclusions and outlook

Variations in the EAWM are strongly associated with the occurrence of severe winter weather, such as cold surges and extreme snowfall. Considering rapid increases in anthropogenic aerosol emissions in Asia over recent decades, we have used the Tsinghua University Community Integrated Earth System Model (CIESM) to investigate the effects of anthropogenic aerosol emissions and concentration changes on the intensity and variability of the EAWM. After confirming that the CIESM captures the mean state of the EAWM well compared with ERA5 reanalysis data (Fig. 2), we show that the net impact of anthropogenic aerosol emissions in this model is to make the EAWM region colder, drier, and snowier (Fig. 4). Average simulated decreases in surface air temperature due to aerosol effects are 1.51°C over southern East Asia and 1.42°C over northern East Asia.

Anthropogenic aerosol emissions strengthen the Siberian High at the surface and extend the East Asian trough northeastward (Fig. 3a-b), consistent with expectations for a stronger EAWM (L. Wang & Chen, 2010; W. Huang et al., 2016; Jiang et al., 2017; Li et al., 2020; Miao & Jiang, 2021). However, anthropogenic aerosols also weaken the East Asian jet in the upper troposphere and shift the Aleutian Low southward at the surface (Fig. 3a,c), changes unlike those associated with strong EAWM periods in the current climate. These seemingly contradictory results are nonetheless in line with previous studies having shown that the vertical structure of the EAWM response to anthropogenic forcing is complex (Miao, Wang, Wang, Zhu, & Sun, 2018) and highlight the value of the isentropic PV framework for assessing and attributing changes in the EAWM and other features embedded in the mid-latitude baroclinic zone (W. Huang et al., 2016).

Surface air temperatures over East Asia are consistently colder when anthropogenic aerosol emissions are included (Fig. 4a). These aerosol effects are comparable to 65% of the difference between strong and weak EAWM periods (∼2°C) in the southern part of the domain and 38% of the difference between strong and weak EAWM periods (∼2.5°C) in the northern part of the domain (Fig. 5). The mechanisms behind these reductions in surface air temperature are distinct between the region southeast of the Tibetan Plateau and the Yangtze River Valley. To the southeast of the Tibetan Plateau, aerosol-cloud interactions and associated changes in diabatic heating produce an anticyclonic circulation anomaly. Upslope southerly flow along the western side of this anomaly intensifies adiabatic cooling, increases cloud cover, and reduces surface shortwave heating (Figs. 7–10), contributing to colder temperatures and significant increases in snowfall along the southeastern flank of the Tibetan Plateau (Fig. 4c). By contrast, the anomalous anticyclone suppresses convection over the Yangtze River Valley, intensifies southward advection of cold air outflow from the Siberian High along the coastal regions of East Asia, and increases clear-sky longwave cooling (Figs. 7–10). These changes are associated with a substantial decrease in total precipitation over land areas in the southern part of East Asia (Fig. 4b).

Previous studies have shown that air quality in central and eastern China typically improves when the EAWM is strong (Ge et al., 2019). This dichotomy between the aerosol influence (increased aerosol concentrations strengthen the monsoon) and the circulation influence (a stronger monsoon reduces aerosol concentrations) suggests the intriguing possibility that anthropogenic aerosol effects on the circulation of this region may partially self-regulate air pollution episodes. However, distinct seasonal variations in the influence of anthropogenic aerosols on the EAWM (Fig. 1a) indicate that this mechanism, if it exists, may be sensitive to specific details of the background state. Future work should investigate the consistency of this response across models and its potential sensitivity to long-term trends and variability in the Northern Hemisphere wintertime background state.

Open Research Section

Monthly mean outputs from the CIESM model simulations used in this work are available through the AeroCom database (https://aerocom.met.no/FAQ/data_access). This work has used monthly ERA5 products on pressure levels (Hersbach et al., 2023a) and single levels (Hersbach et al., 2023b) from the collections hosted by the Copernicus Climate Data Store (https://cds.climate.copernicus.eu).

Acknowledgments

This work has been supported by the National Natural Science Foundation of China (grant number 42275053, 42205085), the Beijing Natural Science Foundation (grant number IS23121) and Open Fund for the Ministry of Education Key Laboratory for Earth System Modeling (2023). We are grateful to Dr Mian Chin for designing the ACAM and UTLS AeroCom experiments and supporting our participation in these activities. We also thank the European Centre for Medium-Range Weather Forecasts for producing the ERA5 reanalyses and providing access to these products.

References

Ackerman, A. S., Hobbs, P. V., & Toon, O. B. (1995). A Model for Particle Microphysics, Turbulent Mixing, and Radiative Transfer in the Stratocumulus-Topped Marine Boundary Layer and Comparisons with Measurements. *Journal of Atmospheric Sciences*, *52*(8), 1204 – 1236. doi: 10.1175/1520-0469(1995)052⟨1204:AMFPMT⟩2.0.CO;2

Blackmon, M. L., Wallace, J. M., Lau, N.-C., & Mullen, S. L. (1977). An Observational Study of the Northern Hemisphere Wintertime Circulation. *Journal of Atmospheric Sciences*, *34*(7), 1040 – 1053. doi: 10.1175/1520-0469(1977)034⟨1040:AOSOTN⟩2.0.CO;2

Carn, S. (2019). *Multi-satellite volcanic sulfur dioxide l4 long-term global database v3.* Greenbelt, MD, USA. (Accessed: 18 December 2019) doi: 10.5067/MEASURES/SO2/DATA405

Chang, C.-P., Harr, P. A., & Chen, H.-J. (2005). Synoptic Disturbances over the Equatorial South China Sea and Western Maritime Continent during Boreal Winter. *Monthly Weather Review*, *133*(3), 489 – 503. doi: 10.1175/MWR-2868.1

Chang, C.-P., & Lau, K. M. (1982). Short-Term Planetary-Scale Interactions over the Tropics and Midlatitudes during Northern Winter. Part I: Contrasts between Active and Inactive Periods. *Monthly Weather Review*, *110*(8), 933 – 946. doi: 10.1175/1520-0493(1982)110⟨0933:STPSIO⟩2.0.CO;2

Chang, C.-P., & Lau, K. M. W. (1980). Northeasterly Cold Surges and Near-Equatorial Disturbances over the Winter MONEX Area During December 1974. Part II: Planetary-Scale Aspects. *Monthly Weather Review*, *108*(3), 298 – 312. doi: 10.1175/1520-0493(1980)108⟨0298:NCSANE⟩2.0.CO;2

Chang, C. P., Wang, Z., & Hendon, H. (2006). The Asian winter monsoon. In *The Asian Monsoon* (pp. 89–127). Berlin, Heidelberg: Springer Berlin Heidelberg. doi: 10.1007/3-540-37722-0_3

Chen, H., & Zhang, Y. (2013). Sensitivity experiments of impacts of large-scale urbanization in East China on East Asian winter monsoon. *Chinese Science Bulletin*, *58*, 809 – 815. doi: https://doi.org/10.1007/s11434-012-5579-z

Compo, G. P., Kiladis, G. N., & Webster, P. J. (1999). The horizontal and vertical structure of east Asian winter monsoon pressure surges. *Quarterly Journal of the Royal Meteorological Society*, *125*(553), 29–54. doi: 10.1002/qj.49712555304

Ding, Y., Ren, G., Zhao, Z., Xu, Y., Luo, Y., Li, Q., & Zhang, J. (2007). Detection, causes and projection of climate change over China: An overview

of recent progress. *Advances in Atmospheric Sciences*, *24*, 954 – 971. doi: 10.1007/s00376-007-0954-4

Fan, K. (2009). Predicting Winter Surface Air Temperature in Northeast China. *Atmospheric and Oceanic Science Letters*, *2*(1), 14–17. doi: 10.1080/16742834.2009.11446770

Ge, W., Yin, Y., Wright, J. S., Huang, W., Jia, B., Wang, Y., & Yang, Z. (2019). Links Between the Large-Scale Circulation and Daily Air Quality Over Central Eastern China During Winter. *Journal of Geophysical Research: Atmospheres*, *124*(13), 7147–7163. doi: 10.1029/2018JD030154

Guo, L., Highwood, E. J., Shaffrey, L. C., & Turner, A. G. (2013). The effect of regional changes in anthropogenic aerosols on rainfall of the East Asian Summer Monsoon. *Atmospheric Chemistry and Physics*, *13*(3), 1521–1534. doi: 10.5194/acp-13-1521-2013

Guo, Q. (1994). Relationship Between the Variations of East Asian Winter Monsoon and Temperature Anomalies China. *Journal of Applied Meteorological Science*, *5*(19940238), 218–225.

He, S., & Wang, H. (2012). An Integrated East Asian Winter Monsoon Index and Its Interannual Variability. *Chinese Journal of Atmospheric Sciences*, *36*(20120307), 523. doi: 10.3878/j.issn.1006-9895.2011.11083

Hersbach, H., Bell, B., Berrisford, P., Biavati, G., Horányi, A., Muñoz Sabater, J., ... Thépaut, J.-N. (2023a). *ERA5 monthly data on pressure levels from 1940 to present.* Copernicus Climate Change Service (C3S) Climate Data Store (CDS). doi: 10.24381/cds.6860a573

Hersbach, H., Bell, B., Berrisford, P., Biavati, G., Horányi, A., Muñoz Sabater, J., ... Thépaut, J.-N. (2023b). *ERA5 monthly data on single levels from 1940 to present.* Copernicus Climate Change Service (C3S) Climate Data Store (CDS). doi: 10.24381/cds.f17050d7

Hersbach, H., Bell, B., Berrisford, P., Hirahara, S., Horányi, A., Muñoz-Sabater, J., ... Thépaut, J.-N. (2020). The ERA5 global reanalysis. *Quarterly Journal of the Royal Meteorological Society*, *146*(730), 1999–2049. doi: 10.1002/qj.3803

Hoesly, R. M., Smith, S. J., Feng, L., Klimont, Z., Janssens-Maenhout, G., Pitkanen, T., ... Zhang, Q. (2018). Historical (1750–2014) anthropogenic emissions of reactive gases and aerosols from the community emissions data system (ceds). *Geoscientific Model Development*, *11*(1), 369–408. doi: 10.5194/gmd-11-369-2018

Hori, M. E., & Ueda, H. (2006). Impact of global warming on the East Asian winter monsoon as revealed by nine coupled atmosphere-ocean GCMs. *Geophysical Research Letters*, *33*(3), L03713. doi: 10.1029/2005GL024961

Hoskins, B. J., McIntyre, M. E., & Robertson, A. W. (1985). On the use and significance of isentropic potential vorticity maps. *Quarterly Journal of the Royal Meteorological Society*, *111*(470), 877–946. doi: https://doi.org/10.1002/qj.49711147002

Hu, Z.-Z., Bengtsson, L., & Arpe, K. (2000). Impact of global warming on the Asian winter monsoon in a coupled GCM. *Journal of Geophysical Research: Atmospheres*, *105*(D4), 4607–4624. doi: 10.1029/1999JD901031

Huang, R., Chen, J., & Huang, G. (2007). Characteristics and variations of the East Asian monsoon system and its impacts on climate disasters in China. *Advances in Atmospheric Sciences*, *24*, 993–1023. doi: 10.1007/s00376-007-0993-x

Huang, R., Zhou, L., & Wen, C. (2003). The Progresses of Recent Studies on the Variabilities of the East Asian Monsoon and Their Causes. *Advances in Atmospheric Sciences*, *20*(1), 55–69. doi: 10.1007/BF03342050

Huang, W., Chen, R., Wang, B., Wright, J. S., Yang, Z., & Ma, W. (2017). Potential vorticity regimes over East Asia during winter. *Journal of Geophysical Research: Atmospheres*, *122*(3), 1524–1544. doi: 10.1002/2016JD025893

Huang, W., Wang, B., & Wright, J. S. (2016). A potential vorticity-based index

for the East Asian winter monsoon. *Journal of Geophysical Research: Atmospheres*, *121*(16), 9382–9399. doi: 10.1002/2016JD025053

Hurrell, J. W., Hack, J. J., Shea, D., Caron, J. M., & Rosinski, J. (2008). A new sea surface temperature and sea ice boundary dataset for the community atmosphere model. *Journal of Climate*, *21*(19), 5145–5153. doi: 10.1175/2008JCLI2292.1

IPCC. (2021). *Climate change 2021: The physical science basis. contribution of working group i to the sixth assessment report of the intergovernmental panel on climate change* (Vol. In Press) [Book]. Cambridge, United Kingdom and New York, NY, USA: Cambridge University Press. doi: 10.1017/9781009157896

Jhun, J.-G., & Lee, E.-J. (2004). A New East Asian Winter Monsoon Index and Associated Characteristics of the Winter Monsoon. *Journal of Climate*, *17*(4), 711 – 726. doi: 10.1175/1520-0442(2004)017⟨0711:ANEAWM⟩2.0.CO;2

Jiang, Y., Liu, X., Yang, X.-Q., & Wang, M. (2013). A numerical study of the effect of different aerosol types on East Asian summer clouds and precipitation. *Atmospheric Environment*, *70*, 51–63. doi: 10.1016/j.atmosenv.2012.12.039

Jiang, Y., Yang, X.-Q., Liu, X., Yang, D., Sun, X., Wang, M., ... Fu, C. (2017). Anthropogenic aerosol effects on East Asian winter monsoon: The role of black carbon-induced Tibetan Plateau warming. *Journal of Geophysical Research: Atmospheres*, *122*(11), 5883–5902. doi: 10.1002/2016JD026237

Lackmann, G. (2012). *Midlatitude Synoptic Meteorology: Dynamics, Analysis, and Forecasting*. Boston, MA, USA: American Meteorological Society. (345pp.)

Lawrence, D. M., Oleson, K. W., Flanner, M. G., Thornton, P. E., Swenson, S. C., Lawrence, P. J., ... Slater, A. G. (2011). Parameterization improvements and functional and structural advances in version 4 of the community land model. *Journal of Advances in Modeling Earth Systems*, *3*(1), M03001. doi: 10.1029/2011MS00045

Lee, S.-S., Kim, S.-H., Jhun, J.-G., Ha, K.-J., & Seo, Y.-W. (2013, jul). Robust warming over East Asia during the boreal winter monsoon and its possible causes. *Environmental Research Letters*, *8*(3), 034001. doi: 10.1088/1748-9326/8/3/034001

Li, J., Carlson, B. E., Yung, Y. L., Lv, D., Hansen, J., Penner, J. E., ... Dong, Y. (2022). Scattering and absorbing aerosols in the climate system. *Nature Reviews Earth & Environment*, *3*, 363–379. doi: 10.1038/s43017-022-00296-7

Li, J., Wang, B., & Yang, Y.-M. (2020). Diagnostic Metrics for Evaluating Model Simulations of the East Asian Monsoon. *Journal of Climate*, *33*(5), 1777–1801. doi: 10.1175/JCLI-D-18-0808.1

Lin, Y., Huang, X., Liang, Y., Qin, Y., Xu, S., Huang, W., ... Gong, P. (2020). Community Integrated Earth System Model (CIESM): Description and Evaluation. *Journal of Advances in Modeling Earth Systems*, *12*(8), e2019MS002036. doi: 10.1029/2019MS002036

Liu, X., Easter, R. C., Ghan, S. J., Zaveri, R., Rasch, P., Shi, X., ... Mitchell, D. (2012). Toward a minimal representation of aerosols in climate models: description and evaluation in the community atmosphere model cam5. *Geoscientific Model Development*, *5*(3), 709–739. doi: 10.5194/gmd-5-709-2012

Liu, Y., Sun, J., & Yang, B. (2009). The effects of black carbon and sulphate aerosols in China regions on East Asia monsoons. *Tellus B*, *61*(4), 642–656. doi: 10.1111/j.1600-0889.2009.00427.x

Luo, X., & Zhang, Y. (2015). The Linkage between Upper-Level Jet Streams over East Asia and East Asian Winter Monsoon Variability. *Journal of Climate*, *28*(22), 9013 – 9028. doi: 10.1175/JCLI-D-15-0160.1

Miao, J., & Jiang, D. (2021). Multidecadal Variations in the East Asian Winter Monsoon and Their Relationship with the Atlantic Multidecadal Oscillation since 1850. *Journal of Climate*, *34*(18), 7525 – 7539. doi:

10.1175/JCLI-D-21-0073.1

Miao, J., Wang, T., Wang, H., & Gao, Y. (2018). Influence of Low-frequency Solar Forcing on the East Asian Winter Monsoon Based on HadCM3 and Observations. *Advances in Atmospheric Sciences*, *35*, 1205 – 1215. doi: 10.1007/s00376-018-7229-0

Miao, J., Wang, T., Wang, H., Zhu, Y., & Sun, J. (2018). Interdecadal Weakening of the East Asian Winter Monsoon in the Mid-1980s: The Roles of External Forcings. *Journal of Climate*, *31*(21), 8985 – 9000. doi: 10.1175/JCLI-D-17-0868.1

Song, F., Zhou, T., & Qian, Y. (2014). Responses of East Asian summer monsoon to natural and anthropogenic forcings in the 17 latest CMIP5 models. *Geophysical Research Letters*, *41*(2), 596–603. doi: 10.1002/2013GL058705

Twomey, S. (1977). The Influence of Pollution on the Shortwave Albedo of Clouds. *Journal of Atmospheric Sciences*, *34*(7), 1149 – 1152. doi: 10.1175/1520-0469(1977)034⟨1149:TIOPOT⟩2.0.CO;2

van Marle, M. J. E., Kloster, S., Magi, B. I., Marlon, J. R., Daniau, A.-L., Field, R. D., ... van der Werf, G. R. (2017). Historic global biomass burning emissions for cmip6 (bb4cmip) based on merging satellite observations with proxies and fire models (1750–2015). *Geoscientific Model Development*, *10*(9), 3329–3357. doi: 10.5194/gmd-10-3329-2017

Wang, B., Wu, R., & Fu, X. (2000). Pacific–East Asian Teleconnection: How Does ENSO Affect East Asian Climate? *Journal of Climate*, *13*(9), 1517 – 1536. doi: 10.1175/1520-0442(2000)013⟨1517:PEATHD⟩2.0.CO;2

Wang, B., Wu, Z., Chang, C., Liu, J., Li, M., & Zhou, T. (2010). Another look at interannual-to-interdecadal variations of the east asian winter monsoon: the northern and southern temperature modes. *Journal of Climate*, *23*, 1495–1512. doi: 10.1175/2009jcli3243.1

Wang, H., Yu, E., & Yang, S. (2011). An exceptionally heavy snowfall in Northeast china: large-scale circulation anomalies and hindcast of the NCAR WRF model. *Meteorology and Atmospheric Physics*, *113*, 11 – 25. doi: 10.1007/s00703-011-0147-7

Wang, L., & Chen, W. (2010). How well do existing indices measure the strength of the East Asian winter monsoon? *Advances in Atmospheric Sciences*, *27*, 855–870. doi: 10.1007/s00376-009-9094-3

Wang, L., Chen, W., Zhou, W., & Huang, R. (2009). Interannual Variations of East Asian Trough Axis at 500 hPa and its Association with the East Asian Winter Monsoon Pathway. *Journal of Climate*, *22*(3), 600 – 614. doi: 10.1175/2008JCLI2295.1

Wei, L., Lu, Z., Wang, Y., Liu, X., Wang, W., Wu, C., ... Jiang, Y. (2022). Black carbon-climate interactions regulate dust burdens over India revealed during COVID-19. *Nature Communications*, *13*, 1839. doi: 10.1038/s41467-022-29468-1

Wu, G., Li, Z., Fu, C., Zhang, X., Zhang, R., Zhang, R., ... Huang, R. (2016). Advances in studying interactions between aerosols and monsoon in China. *Science China Earth Sciences*, *59*, 1 – 16. doi: 10.1007/s11430-015-5198-z

Xu, M., Xu, H., & Ma, J. (2016). Responses of the East Asian winter monsoon to global warming in CMIP5 models. *International Journal of Climatology*, *36*(5), 2139–2155. doi: 10.1002/joc.4480

Yin, J., & Zhang, Y. (2021). Decadal changes of East Asian jet streams and their relationship with the Mid-high Latitude Circulations. *Climate Dynamics*, *56*, 2801–2821. doi: 10.1007/s00382-020-05613-8

Zhang, H., Wang, Z., Wang, Z., Liu, Q., Gong, S., Zhang, X., ... Li, L. (2012). Simulation of direct radiative forcing of aerosols and their effects on East Asian climate using an interactive AGCM-aerosol coupled system. *Climate Dynamics*, *38*, 1675 – 1693. doi: 10.1007/s00382-011-1131-0

766 Zhou, L.-T. (2011). Impact of East Asian winter monsoon on rainfall over south-
767 eastern China and its dynamical process. *International Journal of Climatology*,
768 *31*(5), 677–686. doi: 10.1002/joc.2101
769 Zhou, L.-T., & Wu, R. (2010). Respective impacts of the East Asian winter mon-
770 soon and ENSO on winter rainfall in China. *Journal of Geophysical Research:*
771 *Atmospheres*, *115*(D2), D02107. doi: 10.1029/2009JD012502